Magn Reson Med Sci 2022; 21; 499–515
doi:10.2463/mrms.mp.2021-0007 Published Online: July 22, 2021

MAJOR PAPER

# Diffusion MR Imaging with T2-based Water Suppression (T2wsup-dMRI)

Tokunori Kimura[1*], Kousuke Yamashita[1], and Kouta Fukatsu[1]

**Purpose:** This study proposes and assesses a new diffusion MRI (dMRI) technique to solve problems related to the quantification of parameter maps (apparent diffusion coefficient [ADC] or mean diffusivity [MD], fractional anisotropy [FA]) and misdrawing of fiber tractography (FT) due to cerebrospinal fluid (CSF)-partial volume effects (PVEs) for brain tissues by combining with the T2-based water suppression (T2wsup) technique.

**Methods:** T2wsup–diffusion-weighted imaging (DWI) images were obtained by subtracting those images from the acquired multi-*b* value (*b*) DWI images after correcting the signal intensities of multiecho time (TE) images using long TE water signal-dominant images. Quantitative parameter maps and FT were obtained from minimum data points and were compared with those using the standard (without wsup) DWI method, and partly compared with those obtained using other alternative DWI methods of applying fluid attenuation inversion recovery (FLAIR), non-*b*-zero (NBZ) by theoretical or noise-added simulation and MR images.

**Results:** In the T2wsup-dMRI method, the hyperintense artifacts due to CSF-PVEs in MRI data were dramatically suppressed even at lower $b$ ($\lesssim$ 500 s/mm$^2$) while keeping the tissue SNR. The quantitative parameter map values became precisely close to the pure tissue values precisely even in water (CSF) PVE voxels in healthy brain tissues (T2 $\lesssim$ 100 ms). Furthermore, the fiber tracts were correctly connected, particularly at the fornix in closest contact to the CSF.

**Conclusion:** Solving the problem of CSF-PVE in the current dMRI technique using our proposed T2wsup-dMRI technique is easy, with higher SNR than those obtained with FLAIR or NBZ methods when applying to healthy brain tissues. The proposed T2wsup–dMRI could be useful in clinical settings, although further optimization of the pulse sequence and processing techniques and clinical assessments are required, particularly for long T2 lesions.

**Keywords:** *diffusion-weighted imaging, diffusion tensor imaging, water suppression, partial volume effects, cerebrospinal fluid*

## Introduction

The diffusion magnetic resonance imaging (dMRI) technique, including diffusion-weighted imaging (DWI) and diffusion tensor imaging (DTI), has the potential to provide biomarkers of tissue variation, such as cell density, tissue anisotropy, and microvascular perfusion.[1,2] The dMRI has now being regularly implemented in commercial MRI scanners and is being widely used, particularly in the neurological region related to brain stroke, tumor characterization, and neurodegenerative diseases. The dMRI can provide several quantitative parameter maps, including a diffusivity given by apparent diffusion coefficient (ADC) or mean diffusivity (MD) and diffusion anisotropy given by fractional anisotropy (FA) or relative anisotropy (RA), and it can visualize a fiber tractography (FT) to assess neural tracts. Those are calculated using multiple images acquired using different encoding ranges and directions of diffusion denoted by *b*-values (*b*).

However, a significant limitation of the dMRI technique is the imaging artifacts, which is essential for identifying tissue neural signatures of diseases and brain–behavior relationships.[3–7] In dMRI, it is extremely important to

[1]Department of Radiological Science, Shizuoka College of Medical Care Science, Hamamatsu, Shizuoka, Japan

*Corresponding author: Department of Radiological Science, Shizuoka College of Medical Care Science, 2000, Hirakuchi, Hamakita-ku, Hamamatsu, Shizuoka 434-0041, Japan. Phone: 053-585-1551, e-mail: enocolo.tk@gmail.com, kimura@shiz-med-sci.ac.jp



Received: January 14, 2021 | Accepted: May 21, 2021

suppress the cerebrospinal fluid (CSF) because the quantitative parameter maps are affected by a partial volume effect (PVE) when the CSF is mixed with the brain's gray matter (GM) or white matter (WM) in the same voxel. This is because the standard dMRI (Std-dMRI) images are usually acquired using T2-weighted spin-echo (SE) with longer TE (=80–100 ms) conditions based on single-shot echo-planar imaging (EPI), and because the ADC for the CSF is several times greater than those for brain tissues. The CSF also provides isotropic diffusion. Therefore, compared with pure tissue volumes, the voxel with CSF-PVE introduces an overestimation of ADC, underestimation of anisotropy indexes of FA or RA, and misdrawing in FT.[4–6] To solve these problems, various CSF suppression techniques for dMRI have been proposed and assesed.[8–24]

The first approach is to combine dMRI with a fluid attenuation inversion recovery (FLAIR) sequence to suppress CSF-PVE while using the same range of $b$ as the Std SE sequence, including zero.[5] The FLAIR technique succeeded in providing pure tissue maps of diffusivity and anisotropy even at the tissue-CSF border[8–12] and visualizing tracts, such as the fornix and corpus callosum in closest contact to the CSF in the lateral ventricle.[14,16] Despite these contributions, compared with the Std method without inversion, FLAIR approaches have issues in reducing SNR[14] because of the small longitudinal magnetization ($Mz$), particularly in the high magnetic field due to T1 extension. This could result in an extension of imaging time or reduction in the number of slices and instability due to CSF inflow artifacts, thereby not providing information about the CSF.

The second approach is the non-$b$-zero (NBZ) method,[16,17] in which a greater minimum $b$, $b_{min}$ is used to sufficiently reduce water signals because CSF contamination was a source of non-mono exponential decay even in a GM distant from CSF that could be suppressed by removing the $b \sim 0$ data. For example, in the case of Salminen,[16] $b_{min}$ = 680 s/mm$^2$ was used with a TR = 7.8 s and an TE = 86 ms. In the case of Baron,[17] TR optimization was additionally combined with NBZ method, ($b_{min}$ = 425 s/mm$^2$ with a shorter TR = 2.5 s and TE = 60 ms). Those methods require no model compartment assumption and used the same analysis method as the Std method. However, the NBZ method requires several motion probing gradient (MPG) directions for $b_{min}$ (e.g., minimally three[16] or six[17] to be isotropic but one in the Std DTI). Furthermore, compared with the Std method, it may have the following disadvantages: first, reducing tissue SNR in ADC and FA because the range of $b$ is reduced; and, second, is insufficient water signal suppression depending on the minimum $b$. Thus, this paper assessed these issues.

The third approach is the free-water elimination (FWE) method, in which Std acquisition data are used to analytically separate free water from tissue components.[18–24] The method assumes that two subregions exist within a voxel demonstrating characteristic tensor signals for brain tissue and free water. By calculating separate tensors for the CSF and brain tissue, the FWE method can control CSF contamination. The FWE method has several variations. Two types of methods have been proposed: a single-shell method[18–23] and a multi-shell method.[24–25] The multi-shell method can provide better results due to fitting of multiple shells of DWI data, with each shell providing tensor information and having different $b$. Pasternak et al.[18] showed that their single-shell, bi-tensor model-based FWE technique could separate free water and WM in edema and increase the FA value compared with in the Std DTI method.[18] Their technique is beginning to be used clinically.[19–26] However, the FWE method requires many data points with non-zero $b$ for multi-shell method, MPG directions, and complicated analysis based on a model assumption.

On the other hand, several computational imaging techniques, including computed DWI or synthetic MRI, have been proposed to provide several quantification parameter maps (e.g., T2, T1, proton density [PD], and ADC maps). The images obtained using these techniques are combined with the weighted images, which are difficult to acquire directly due to hardware limitation or noise effects.[26–29] DWI images with high $b$ and high contrast-to-noise ratio can be obtained using the ADC maps calculated by combining DWI images with relatively lower $b$.[26,27] As for derivative methods, a short TE DWI method including zero TE was proposed by additionally using T2 maps,[29] which can reduce T2 shine-through effects,[30] and a method to provide FLAIR–DWI images with higher SNR was proposed by additionally using T1 maps.[31] Furthermore, a new synthetic imaging technique was proposed on the basis of the proposed T2-based water-suppression (T2wsup)[32] method (a modified version of the high-intensity reduction [HIRE] technique[33]), which provides synthetic FLAIR or SE images that are free of hyperintense artifacts due to CSF-PVE problematic in conventional synthetic MRI method.[34–35]

This study assesses the effectiveness of proposed wsup technique for dMRI called T2wsup-dMRI in solving the problems existing in several conventional approaches by combining with the proposed T2wsup technique.

## Materials and Methods

### *Signal model*

Here, we assume that a single voxel in a brain MRI SE image is modeled by a two-compartment model, in which the single voxel includes two components of water and tissue, and each of the components is described as a single-compartment model with a single T2 relaxation time and with Gaussian diffusion ellipsoid representation of a single tensor model.[1,2] In addition, the T2 and ADC in CSF are assumed to be constant in the entire brain, the motion effects are negligible, and MRI SE image acquired with very long TE can be regarded as a water signal dominant, where the signal intensities (SIs) over a certain threshold are assumed to be from pure (100%) water.

Figure 1 shows a schematic diagram of a two-compartment model for SE DWI signal with $TE$ and $b$-factor, $b$, SI, and $S(TE, b)$ in a single voxel. The $S(TE, b)$ is a mixture of

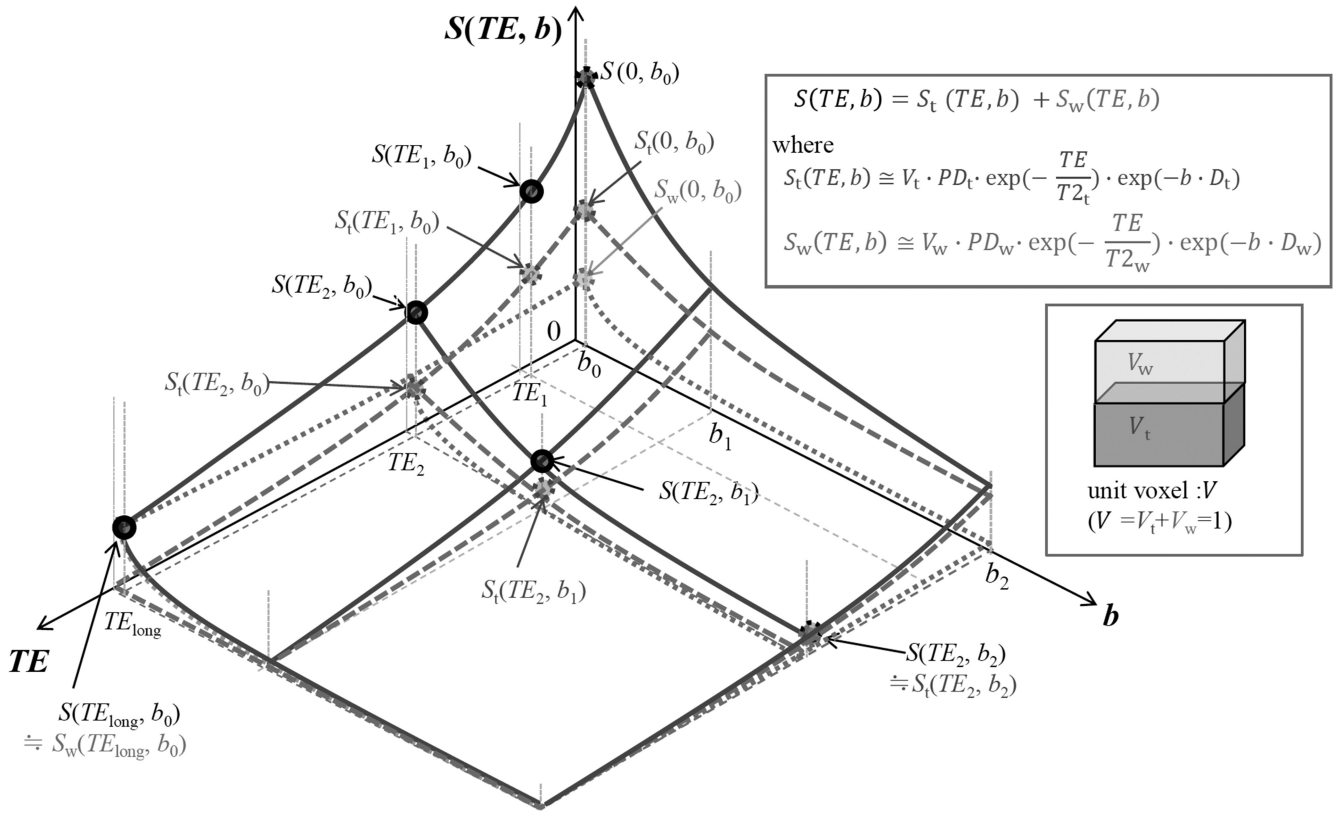


**Fig. 1** Schematic of DWI signal space, *S*(*TE, b*), assuming a two-compartment model that contains tissue and water in a unit voxel. The gray dashed line means tissue signal, $S_t$; thin gray dotted line means water signal, $S_w$; and black solid line means total signal, $S = S_w + S_t$. The minimum number of data points to obtain $T2_t$ and $D_t$ is four points of $S(TE_1, b_0)$, $S(TE_2, b_0)$, $S(TE_3, b_0)$, and $S(TE_2, b_1)$, where $TE_3$ is selected as water signal dominant ($TE_3 = TE_{long}$). Obtaining only the $D_t$ requires three points, except for $S(TE_1, b_0)$. Besides, several directions of MPGs are required as $b_1$ to obtain diffusion directions; for example, three points for isotropic DWI and ADC or six points for DTI. Here TR is asssmed to be long enough and constant. *b*, b-value; *D*, apparent diffusion coefficient (ADC); DTI, diffusion tensor imaging; DWI, diffusion-weighted imaging; MPG, motion probing gradient; *PD*, proton density; *S*, signal intensity; t, tissue; *T2*, transverse relaxation time; *V*, unit voxel volume; *w*, water.

tissue SI, $S_t$ (*TE, b*), and water SI, $S_w$ (*TE, b*), given using the following equation:

$$S_i(TE, b) = S_{w_i}(TE, b) + S_{t_i}(TE, b) \tag{1}$$

where subscripts w, t, and *i* are water, tissue compartment, and MPG direction, respectively. Water and tissue SIs are obtained using the following equation adding MPG direction:

$$S_{w_i,t_i}(TE,b) = Mz_{w,t} \cdot DecayT2_{w,t} \cdot DecayD_{w_i,t_i} \tag{2}$$

where

$$Mz_{w,t} = V_{w,t} \cdot PD_{w,t} \cdot DecayT1_{w,t} \tag{3}$$

$$DecayT1_{w,t} = \begin{cases} 1 - \exp\left[-TR/T1_{w,t}\right] & (SE) \\ 1 - 2 \cdot \exp\left[-TI/T1_{w,t}\right] + \exp\left[-TR/T1_{w,t}\right] & (FLAIR) \end{cases} \tag{4}$$

$$DecayT2_{w,t} = \exp\left[-TE/T2_{w,t}\right] \tag{5}$$

$$DecayD_{w_i,t_i} = \exp\left[-b_i \mathbf{g}_i^T \mathbf{D}_{w,t}\, \mathbf{g}_i\right] \tag{6}$$

where $Mz_{w,t}$ is the water or tissue longitudinal magnetization, $V_{w,t}$ is the water or tissue volume in unit voxel $V$ ($V = V_w + V_t = 1$), $PD_{w,t}$ is the water or tissue PD, $T2_{w,t}$ is the water or tissue transverse relaxation time, $T1_{w,t}$ is the water or tissue longitudinal relaxation time, and $b_i$ and $\boldsymbol{g}_i$ are the diffusion-weighting amplitude (b-value) (in s/mm$^2$) and unit gradient encoding vector, respectively, and $\mathbf{D}_{w,t}$ is the water or tissue diffusion tensor, described by

$$\mathbf{D} = \begin{pmatrix} D_{xx} & D_{xy} & D_{xz} \\ D_{yx} & D_{yy} & D_{yz} \\ D_{zx} & D_{zy} & D_{zz} \end{pmatrix} \tag{7}$$

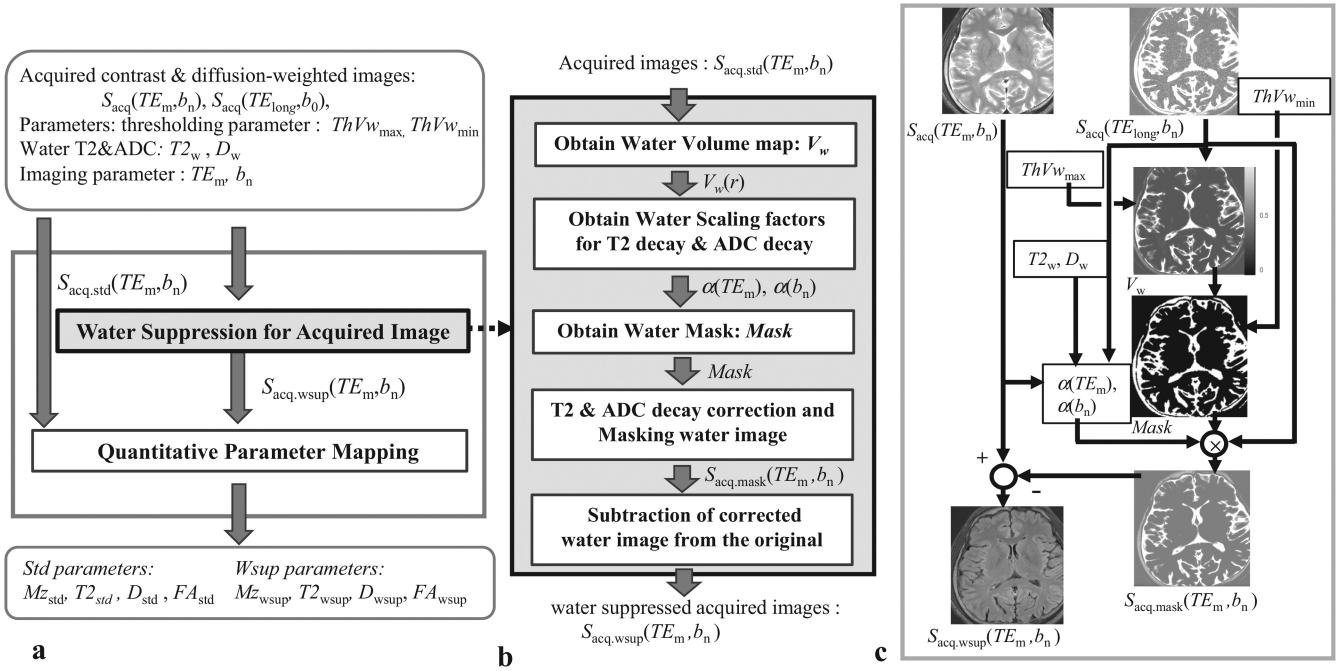


**Fig. 2** Process flow for the currently proposed technique of T2wsup-dMRI. General whole process (**a**), detailed process for water suppression for the acquired image (**b**), and the process flow **b** shown with typical output images in each process using $b = 0$ images (**c**), where TR and TI in process **b** are abbreviated because those are common. *b*, b-value; DWI, diffusion-weighted imaging; TI, inversion time.

### *T2wsup*

Here, we consider the problems associated with simply obtaining DWI images and parameter maps of only tissue components by eliminating water components. To reduce the CSF-PVE in the acquired DWI images, we used the T2wsup technique,[32] a modified version of the HIRE technique.[33] The basic flow for T2wsup for an image with $b = 0$ ($b_0$) image is almost similar to that reported by Kimura et al.[32] We used a Std SE–DWI sequence for imaging.

For imaging, we acquired Std images of $b = b_0$ (~0) with $TE = TE_m$ ($m = 1, \ldots, M$) at spatial position $r$ in all imaging spaces $R$, $S_{acq}(TE_m, b_0, r)$ and DWI images of $b_n > 0$ ($n = 1, 2, \ldots, N$) with the same TE, $S_{acq}(TE_m, b_n, r)$, images of $b = b_0$ with long TE ($TE_M = TE_{long}$) assumed to be pure water (neglecting tissue) signals, $S_{acq}(TE_{long}, b_0, r)$.

Figure 2a shows the general total processing flow of our T2wsup-dMRI technique, and Fig. 2b shows the key flow of wsup for the acquired DWI images, with its example shown in Fig. 2c. The following is the detailed algorithm for the T2wsup-dMRI method:

First, obtain the water volume ratio map, $V_w(r)\ (0 \le V_w(r) \le 1)$ and normalize it by dividing the pure water (CSF) SI in the long TE image, $S_{acq}(TE_{long}, b_0, r)$, in which the easiest way is using a maximum value of the long TE image as follows:

$$S_{acq.\,max}(TE_{long}, b_0) = \max_{r \in R}[S_{acq}(TE_{long}, b_0, r)] \quad (8)$$

$$V_w(r) = \frac{S_{acq}(TE_{long}, b_0, r)}{S_{acq.\,max}(TE_{long}, b_0)} \quad (9)$$

where $\max_{r \in R}[\ ]$ is an operator to obtain the maximum value for all $r$ in $R$. Optionally, it is possible to make it robust by enlarging the pure CSF portion as follows:

$$V_W(r) = \begin{cases} 1 & (S_{acq}(TE_{long}, b_0, r) \ge ThVw_{max}) \\ \dfrac{S_{acq}(TE_{long}, b_0, r)}{ThVw_{max} \cdot S_{acq.\,max}(TE_{long}, b_0)} & (otherwise) \end{cases} \quad (9')$$

where $ThVw_{max}$ is the threshold to be included in the pure CSF portions. If $ThVw_{max} = 1$ in Eq. (9′), then Eq. (9′) becomes Eq. (9).

Second, obtain water scaling factors for T2 decay, $\alpha(TE_m)$, and for ADC decay, $\alpha(b_n)$, to convert SI at the acquired condition of water image, $S_{acq}(TE_{long}, b_0, r)$to the DWI image, $S_{acq}(TE_m, b_n, r)$, as follows.

a) The $\alpha(TE_m)$ is obtained using the T2 of water, $T2_w$, or using the SI ratio at pure CSF portion when the $T2_w$ is unknown, respectively, as

$$\alpha(TE_{\mathrm{m}}) = \exp\left[-\left(TE_{\mathrm{m}} - TE_{\mathrm{long}}\right)/T2_{\mathrm{w}}\right], m = 1, 2, \ldots, M-1 \tag{10}$$

and

$$\alpha(TE_{\mathrm{m}}) = \frac{S_{\mathrm{acq.mean}}(TE_{\mathrm{m}}, b_0)}{S_{\mathrm{acq.mean}}\left(TE_{\mathrm{long}}, b_0\right)} \tag{10'}$$

where

$$S_{\mathrm{acq.mean}}\left(TE_{\mathrm{m,\,long}}, \mathrm{b}_0\right) = \underset{r' \in V_{\mathrm{w}}(r)=1}{\mathrm{mean}} \left[S_{\mathrm{acq}}\left(\mathrm{TE}_{\mathrm{m,\,long}}, b_0, r\right)\right]$$

and $\underset{r \in V_{\mathrm{w}}(r)=1}{\mathrm{mean}}[\ ]$ is an operator to obtain the averaged value for all $r$ satisfying $r \in V_{\mathrm{w}}(r) = 1$.

b) The $\alpha(b_{\mathrm{n}})$ is obtained using water ADC, $\boldsymbol{D}_{\mathrm{w}}$, which is measured at stationary pure water (CSF) portions or assumed to be isotropic ($D_{\mathrm{xx}} = D_{\mathrm{yy}} = D_{\mathrm{zz}} = D_{\mathrm{w}}$) and literature value of approximately $3.0 \times 10^{-3}$ mm$^2$/s as follows:

$$\alpha(b_{\mathrm{n}}) = \exp[-(b_{\mathrm{n}} - b_0)D_{\mathrm{w}}] \tag{11}$$

Third, obtain a spatial mask, $Mask(r)$,to keep the SNR of tissue portions after subtraction as follows:

$$Mask(r) = \begin{cases} 1 & (V_{\mathrm{w}}(r) \geq ThVw_{\mathrm{min}}) \\ 0 & (otherwise) \end{cases} \tag{12}$$

where $ThVw_{\mathrm{min}}$ is a threshold value (0–1) when pure (100%) water is 1 and decided experimentally, dependent on $TE_{\mathrm{long}}$; however, it can be commonly used once it is decided. Then, a spatial smoothing filter is applied to the $Mask(r)$ to smooth the boundary of 0 and 1 in the mask.

Fourth, obtain water images after SI correction from $(TE_{\mathrm{long}}, b_0)$ to $(TE_{\mathrm{m}}, b_{\mathrm{n}})$ and masking from the standard $b_0$ images as follows:

$$\begin{aligned} S_{\mathrm{acq.mask}}(TE_{\mathrm{m}}, b_{\mathrm{n}}, r) = {} & Mask(r) \cdot \alpha(TE_{\mathrm{m}}) \cdot \alpha(b_{\mathrm{n}}) \\ & \cdot S_{\mathrm{acq.mask}}(TE_{\mathrm{long}}, b_0, r) \end{aligned} \tag{13}$$

Finally, our proposed water-suppressed DWI (T2wsup DWI) images, $S_{\mathrm{acq.wsup}}(TE_{\mathrm{m}}, b_{\mathrm{n}}, r)$, are obtained by subtracting the corrected water images with the same TE and $b$ in Eq. (13) as follows:

$$\begin{aligned} S_{\mathrm{acq.wsup}}(TE_{\mathrm{m}}, b_{\mathrm{n}}, r) = {} & S_{\mathrm{acq}}(TE_{\mathrm{m}}, b_{\mathrm{n}}, r) \\ & - S_{\mathrm{acq.wsup}}(TE_{\mathrm{m}}, b_{\mathrm{n}}, r) \end{aligned} \tag{14}$$

When only the T2wsup DWI images with a single MPG direction are required, the minimum number of data is three ($M$ = 2 and $N$ = 1). In contrast, when it optionally requires synthetic wsup images, except for DWI (i.e., water-suppressed quantitative parameter maps of PD and T2), the minimum required number of data is four ($M$ = 3 and $N$ = 1), as shown in the closed circles in Figure 1.

After obtaining the T2wsup DWI images under the same condition as the standard DWI images, we can obtain the quantitative parameter maps of ADC (MD), FA, and FT using those T2wsup DWI images for the entire range of $b$, including $b$ = 0 by the same way as the Std (w/o wsup) dMRI method.

### *Quantitative parameters in dMRI*

When the DWI images are acquired using the two-point method using the $b$ = and $b$ = data with the same TE and MPG direction, we can calculate the ADC for each direction $i$, $D_i$ as follows:

$$D_i = \frac{\ln[S_i(TE, b_0)/S_i(TE, b_{\mathrm{n}})]}{b_0 - b_{\mathrm{n}}} \tag{15}$$

When using multiple point $b$ SIs ($n$ = 1, 2, …), a linear least-square method is used to obtain $D_i$. In standard clinical DTI,[1,2] an ellipsoid diffusion tensor model is assumed, and the three eigenvalues of DTI tensor ellipsoid, $\lambda_{1,2,3}$ ($\lambda_1 \geq \lambda_2 \geq \lambda_3$), are obtained using a diagonalization process after obtaining DWI images in the laboratory frame ($x$, $y$, $z$) with several MPG directions ($i \geq 6$). Thus, MD and FA can be obtained as follows:

$$MD = \frac{\lambda_1 + \lambda_2 + \lambda_3}{3} = \frac{D_{xx} + D_{yy} + D_{zz}}{3} \tag{16}$$

$$FA = \sqrt{\frac{1}{2}}\sqrt{\frac{(\lambda_1 - \lambda_2)^2 + (\lambda_2 - \lambda_3)^2 + (\lambda_3 - \lambda_1)^2}{\left(\lambda_1^2 + \lambda_2^2 + \lambda_3^2\right)}} \tag{17}$$

where $D_{\mathrm{xx}}$, $D_{\mathrm{yy}}$, and $D_{\mathrm{zz}}$ are diffusion constants obtained at each direction of the laboratory frame ($x$, $y$, $z$). The $MD$ can be obtained from only three-axis measurements ($i$ = 1, 2, 3) because it is obtained only using the diagonal elements of $D_{xx}, D_{yy}$, *and* $D_{zz}$ of 3 × 3 tensor matrix before the diagonalization process, as shown in Eq. (16).

### *SNR of the ADC map*

The SNR of the ADC map with a single MPG direction calculated by the two-point method in Eq. (15) is given as follows.[36–37] The standard deviation (SD) of $D$ (=$D_{\mathrm{i}}$), $\sigma_D$ is obtained by

$$\begin{aligned} \sigma_D^2 &= \sigma_0^2\left(\frac{\delta D}{\delta S(b_0)}\right)^2 + \sigma_{\mathrm{n}}^2\left(\frac{\delta D}{\delta S(b_{\mathrm{n}})}\right)^2 \\ &= \frac{1}{(b_{\mathrm{n}} - b_0)^2}\left[\left(\frac{\sigma_0}{S(b_0)}\right)^2 + \left(\frac{\sigma_{\mathrm{n}}}{S(b_{\mathrm{n}})}\right)^2\right] \end{aligned} \tag{18}$$

Finally, the SNR of $D$ is obtained as

$$SNR(D) = \frac{D}{\sigma_D} = \frac{-\ln\left[\frac{S(b_n)}{S(b_0)}\right]\left[\frac{S(b_0)}{\sigma_0}\right]}{\sqrt{1+\frac{\left(\frac{\sigma_n}{\sigma_0}\right)^2}{\left[\frac{S(b_n)}{S(b_0)}\right]^2}}} \quad (19)$$

where $S(b_0)$ and $S(b_n)$ indicate the SIs of b = $b_0$ and b = $b_n$ images ($b_n > b_0$), $\sigma_0$ and $\sigma_n$ are the SDs of noise in $S(b_0)$ and $S(b_n)$ assuming Gaussian noise.

In Std DWI methods including FLAIR and NBZ methods, the $\sigma_0$ and $\sigma_n$ are independent of $b$, becoming the same as the noise SD in original acquired image, $\sigma$, i.e., $\sigma_0 = \sigma_n = \sigma$. In contrast, in T2wsup-DWI method, the noise SDs become the same as in the Std DWI when the masking process in Eq. (13) was performed. However, when the *Mask* in Eq. (13) is not zero, those become to be

$$\sigma_0 = \sqrt{\{1+\alpha(TE_m)\}}\,\sigma \text{ and } \sigma_n = \sqrt{\{1+\alpha(TE_m)\alpha(b_n)\}}\,\sigma.$$

Note that the $\sigma_n$ becomes close to $\sigma$ with increasing $b_n$ in DWI images even when the masking was not performed.

### *Simulation*

Here, both the theoretical and noise-added simulations were performed. It is assumed in this stimulation that the axes of three MPGs ($i$ = 1, 2, 3) coincide with the three axes of eigenvectors in tensor ellipsoid. Thus, the isotropic diffusion model for water becomes $\lambda_{w1} = \lambda_{w2} = \lambda_{w3}$ and WM of the cylinder tensor model[2] for tissue becomes $\lambda_{t_1}(long\ axis) > \lambda_{t_2}(\text{short } axis) = \lambda_{t_3}$. Therefore, the errors, including SNR changes in diagonalization process in actual DTI process, are not included in our noise-added simulation. Table 1 shows the simulation parameters.

For theoretical simulations, first, the PVE degree was quantitatively compared with the Std (w/o wsup) methods including NBZ and T2wsup methods, and MD and FA were then calculated on the basis of a single-compartment model from the averaged SIs as a parameter of $V_w$. Second, the SIs as a function of $b$ were compared among the three DWI methods, namely, Std, FLAIR, and our T2wsup, each as a parameter of water volume ratio ($V_w$). Third, the SNRs of ADC obtained using Eq. (19) were compared for the four DWI methods assuming the short axis of pure nerve fiber tissue volume ($V_w$ = 0). Furthermore in T2wsup method, the masking effects were compared between with (Mask = 0) and without (Mask = 1).

For noise-added simulations, Gaussian noises of $\sigma$ = 0.029 were added to the SIs and absolute values were taken, where the SNR ($\frac{S(b_0)}{\sigma}$ in Eq. [19]) was 100 at S($b_0$ = 0) of $V_w$ = 0. The mean and SD values were calculated after a trial of 10,000 times to calculate the four tissue parameters of $Mz_t$, $T2_t$, $MD_t$, and $FA_t$. In the T2wsup method based on the proposed algorithm with $ThVw_{min}$ = 0.1, tissue T2, $T2_t$, and water volume, $V_w$ were varied from 0 to 0.9 to assess errors in calculated model parameters. Note that the SNRs for S($b_0$ = 0) in T2wsup method were reduced with increasing $V_w$ due to the tissue SIs are proportional to $V_t$ (=1–$V_w$). Next, the SNRs in pure tissue signals ($V_w$ = 0) with 4 methods, including NBZ method, were compared. For the $S(b_0)$ data, a single datum was used in the Std and T2wsup methods because of $b_0$ = 0, but the different noise-added 3-axes data were used for $b_0$ = 500 and 1000 s/mm$^2$ in the NBZ methods.

### *MRI experiments*

A healthy volunteer study was performed on an MRI machine (Galan 3T ZGO; Canon Medical Systems, Tochigi, Japan) with a 32-channel head coil after obtaining written informed consent. This study was approved by the Institutional Review Board of the Shizuoka College of Medical Care Science (Shizuoka, Japan) and Canon Medical Systems Corp. The SE–EPI sequence was used, in which the common acquisition parameters were as follows: parallel imaging of speed-up factor 3; the number of slices was selected at the maximum for long TE images; the number of average = 1, FOV = 23 cm, acquisition matrix = 192 × 256 (phase encode × read out); display matrix = 512 × 512 after sinc interpolation; and software-based correction of geometric distortion due to eddy current was performed to maintain spatial fidelity. The analysis parameters were as follows: $\alpha(TE)$ was measured using the SI ratio with $ThVw_{max}$ = 1, $D_w$ = 3 × 10$^{-3}$ mm$^2$/s,[16] and experimentally determined $ThVw_{min}$ = 0.1. The two cases of data were assessed with and without our T2wsup technique in each case.

#### Case 1

Three-axis DWI and contrast weighted images: 5 mm × 16 slices; $TR_1$ = 8000 ms; $TE_1$ = 25 ms; $TE_2$ = 80 ms; $TE_{long}$ = 300 ms; $TI$ = 1000 ms; and $b$ = 0, 250, 500, 1000, 1500, and 2000 s/mm$^2$. In addition to synthetic T2wsup images of $b$ = 0, isotropic DWI and isotropic ADC (MD) images were obtained for various $b$ combinations.

#### Case 2

Six-axis DTI: 3 mm × 50 slices; $TR_1$ = 10000 ms; $TE_{long}$ = 500 ms; $TE_2$ = 48 ms; and $b$ = 0, 1000 s/mm$^2$. Isotropic DWI, MD, FA, color FA, and FT images were obtained. T2 maps were additionally calculated from the images with TE=25 and 80 ms. dTV-II.SR and Volume-One v.1.72 (http://medimg.info.hiroshima-cu.ac.jp/dTV.II.15g/) were used for DTI data analysis. Tractography analysis was performed after iso-voxel interpolation to 256 × 256 × 350 (voxel volume = 0.9 mm$^3$), followed by drawing the tracts by

**Table 1** Simulation conditions of quantitative parameters and imaging parameters for 3 water suppression DWI methods

| Quantitative parameter[a)] | Water (CSF) | Tissue (WM) |
|---|---|---|
| *PD* | 0.97 | 0.8 |
| *T1* (ms) | 4000 | 1000 |
| *T2* (ms) | 1910 | 100 |
| $\lambda_1$ (mm$^2$/s) | 3.0 x 10$^{-3}$ | 1.2 x 10$^{-3}$ |
| $\lambda_2$ (mm$^2$/s) | 3.0 x 10$^{-3}$ | 0.6 x 10$^{-3}$ |
| $\lambda_3$ (mm$^2$/s) | 3.0 x 10$^{-3}$ | 0.6 x 10$^{-3}$ |
| *MD* (mm$^2$/s) | 3.0 x 10$^{-3}$ | 0.8 x 10$^{-3}$ |
| *FA* | 0.00 | 0.41 |
| **DWI method** | **Imaging parameters** | |
| T2wsup-DWI | $S(TR_1,TE_1, b_0)$[b)] | |
| | $S(TR_1,TE_2,b_0)$ | |
| | $S(TR_1,TE_3,b_0)$[c)] | |
| | $S(TR_1,TE_2,b_n)$ | |
| | ($b_0$, $b_n$) (s/mm$^2$) | (0, 1500) |
| FLAIR-DWI | $S(TR_1,TI_2,TE_2,b_0)$ | |
| | $S(TR_1,TI_2,TE_2,b_n)$ | |
| | ($b_0$, $b_n$) (s/mm$^2$) | (0, 1500) |
| NBZ-DWI | $S(TR_1,TE_2,b_0)$ | |
| | $S(TR_1,TE_2,b_n)$ | |
| | ($b_0$, $b_n$) (s/mm$^2$) | (500, 1500); (1000,1500) |
| | $TR_1$ (ms) | 10000 |
| | $TE_1$,$TE_2$,$TE_3$ (ms) | 20, 100, 500 |
| | $TI_2$ (ms) | 2350 |

a) quantitative parameters were referred to Ref. #34 and Ref. #23.
b) need for T2, no need for ADC.
c) need for water image, $TE_3$ correspond to $TE_{long}$.
CSF, cerebrospinal fluid; DWI, diffusion-weighted imaging; FA, fractional anisotropy; FLAIR, fluid attenuation inversion recovery; MD, mean diffusivity; NBZ, non-*b*-zero; PD, proton density; T2wsup, T2-based water suppression; WM, white matter.

setting two seed ROIs on the portion of the fornix crus with the threshold parameters of FA to stop drawing commonly at 0.25.

## Results

### *Simulation*

Figures 3–6 and Table 2 show the simulation results. For the DTI quantitative parameter maps of MD and FA as a function of $V_w$ (Fig. 3), the Std DWI method became close to each pure water value with increasing $V_w$. Larger $b_0$ values corresponding to the NBZ–DWI method reduced water effects but were not sufficient even at $b_0$ = 1000 s/mm$^2$. In contrast, the MD and FA with the T2wsup were kept constant with the ground truth tissue values being independent of $V_w$, except when $V_w$ was 100%.

For the SIs as a function of *b* for three DWI methods, each as a parameter of water volume ratio ($V_w$) (Fig. 4), the Std method provided bi-exponential decay for $V_w$ = 25%–75%. The water components were relatively reduced by increasing *b* but remained at a *b* of 1000. In contrast, the FLAIR method and our proposed T2wsup method provided the SI decay of pure tissue component thorough the entire *b*, and those SIs were proportional to tissue volume ($V_t = 1 - V_w$), whereas the SIs in T2wsup–DWI were 24% better than those in FLAIR–DWI, reflecting a difference in SI ($b = 0$).

For the theoretical SNRs of the ADC values of pure tissue as a function of $b_n$ for three DWI techniques using the two-point method (Fig. 5), the Std SE method (Std($b_0$ = 0)) and our T2wsup with masking method provided the best performance through the entire range of $b_n$.

Our noise-added simulation results at $b_n$ = 1500 s/mm$^2$ in pure tissues ($V_w$ = 0) (Table 2) provided almost the same SNRs between the T2wsup and the Std because the subtraction processes were eliminated in our T2wsup method due to the thresholding effects when $V_w < ThVw_{min}$. The SNRs in NBZ method were lower than the Std or T2wsup methods. Those results were almost the same as in the theoretical simulation in Fig. 5.

For noise-added simulation with the T2wsup method (Fig. 6), the errors in the quantitative parameters at $T2_t$ = 100 ms were reasonable, but the errors for $V_w$ = 10–90% became greater as the $T2_t$ became longer (closer to $TE_{long}$) since the components of tissue SIs were relatively greater with increasing $T2_t$ at TE = $TE_{long}$ and could not be sufficiently separated in our current T2wsup-dMRI algorithm. In this simulation, the SDs were kept $\sigma = 0.0029$ (SNR = 100 at $T2_t$ = 100 ms) corresponding original added noise at $V_w$ = 10% but the SDs were increased to $\alpha(TE) = 1.5\sigma = 0.0043$ at $V_w \geq 25\%$ for $T2_t$ = 100–150 ms. The SDs in T2wsup SIs at $V_w$ = 10% for $T2_t$ = 100–150 ms and $V_w$ = 0% for $T2_t$ = 200 ms were further increased due to the instability of the thresholding (mixed with or without subtraction in trials) in the current algorithm. Those errors were transformed to the errors in quantitative parameters calculated afterwards.

Anyway, these simulation results indicate that the Std-dMRI along with wsup technique, that is, T2wsup-dMRI, provides the best results among the three methods evaluated in terms of both SNR and wsup effects.

### *MRI experiments*

Figure 7–8 and Table 3 show the results of case 1. Comparing the DWI images with the Std method and those with our T2wsup method (Fig. 7a), the CSF signals for T2wsup

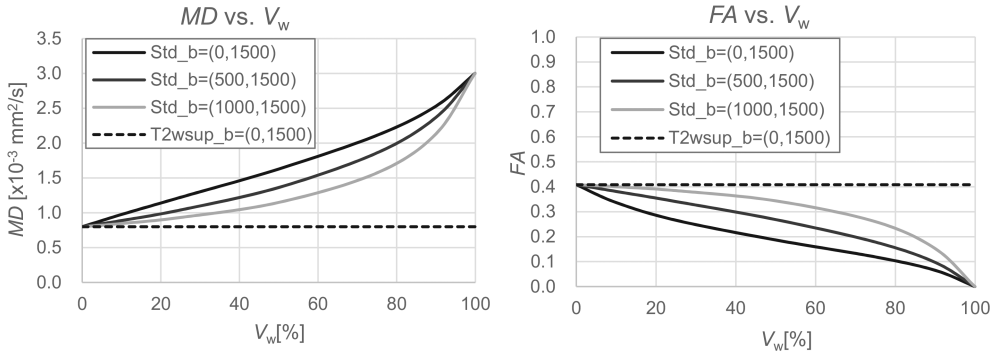


**Fig. 3** Theoretical simulation results of *MD* and *FA* as a function of $V_w$ (%) for standard (w/o wsup) DWI (Std) and T2-based water suppression DWI (T2wsup) obtained by the two-point method for WM with denoted combinations of $b = (b_0, b_n)$ *s/mm*$^2$. Note that the *MD* and *FA* for standard respectively increased and decreased with the increasing $V_w$. The greater $b_0$ values corresponding to the NBZ-DWI reduced water effects but were not sufficient even at $b_0$ = 1000 s/mm$^2$. In contrast, the *MD* and *FA* with T2wsup-DWI were kept constant to the theoretical tissue values (*MD* = 0.8 × 10$^{-3}$ mm$^2$/s, *FA* = 0.41) through whole $V_w$, expect for $V_w$ = 100% (no tissue signal). Simulation parameters were shown in Table 1. *b*, b-value; DWI, diffusion weighted imaging; *FA*, fractional anisotropy; *MD*, mean diffusivity; NBZ, non-*b*-zero; Std, standard; T2wsup, T2-based water suppression.

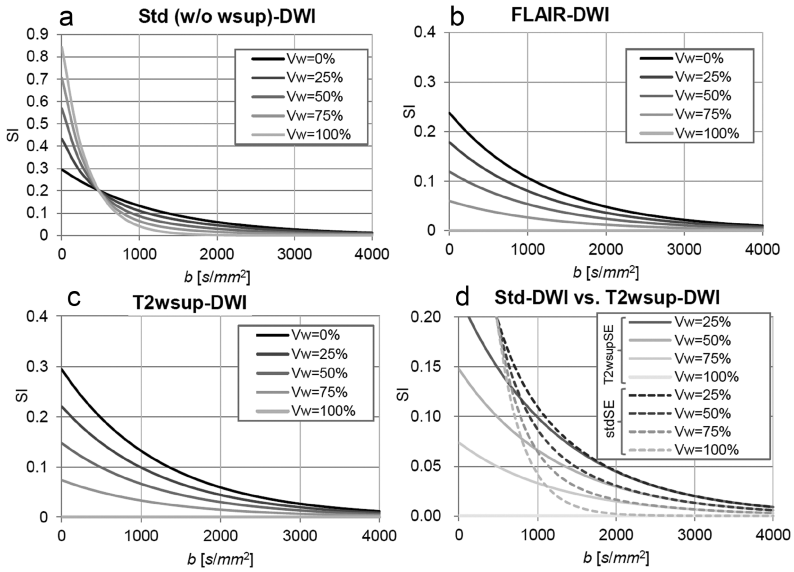


**Fig. 4** Theoretical simulation results of SIs as a function of *b* for three DWI methods (**a**–**c**) each as a parameter of water volume ratio ($V_w$), and overlapped version of the Std (w/o wsup) and T2wsup DWI methods with magnification (**d**). *b*, b-value; FLAIR, fluid attenuation inversion recovery; DWI, diffusion-weighted imaging; Std, standard; T2wsup, T2-based water suppression.

were well suppressed in the entire range of *b*, including *b* = 0, particularly in the CSF-PVE portions, such as the cerebral cortex and cerebellum. The CSF signals remained constant until a *b* of 1000 s/mm$^2$ for the Std method. The CSF signals, such as those in the Monro foramen at a *b* of 250–500 s/mm$^2$ for the Std method, were lower than those in the lateral ventricle because of the effects of CSF. Therefore, the CSF signals for T2wsup were negative because of the overestimation of subtracted CSF signals (underestimation of the estimated $D_w$) at those portions. Comparing the characteristics of ln[S(b)] with *b* (Fig. 7b), those in the cerebellum and temporal portions for the Std method were not linear because of CSF-PVE. In contrast, those for the T2wsup method had higher linearity, and the gradients corresponding to ADC (MD) values became close to the pure tissue values even at the ROIs, including CSF and tissue (Table 3).

Figure 8 shows the contrast-enhanced weighted images and the quantitative parameter maps for the Std (without wsup) and the currently proposed T2wsup methods. Comparing the ADC (MD) values for the T2wsup (*b* = 0, 1500) with those for NBZ (*b* = 500, 1500), the tissue SNRs and CSF suppression effects for the current method were greater compared with those for the NBZ. The SNR measured at the uniform tissue portions in the MD map

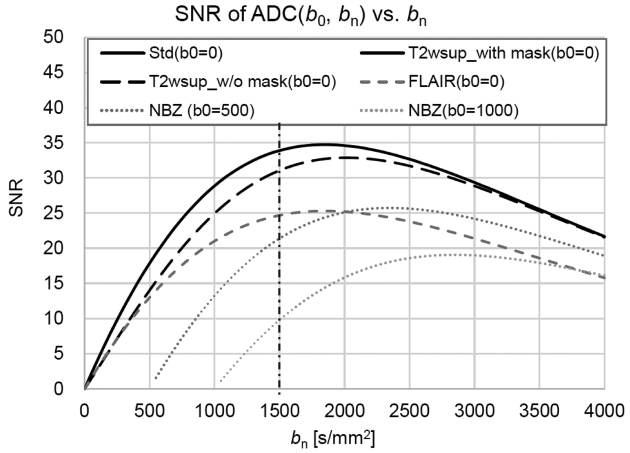


**Fig. 5** Theoretical SNRs of ADC values as a function of the second $b$, $b_n$ of pure tissue ($V_w$ = 0, $D_t$ = 0.6 × $10^{-3}$ mm$^2$/s) for five DWI techniques using the two-point method when the SNR of SE $b_0$ SI (Std[$b$=$b_0$]) for $V_w$ = 0 (S($b_0$)/$\sigma_0$ = 100. The NBZ method was shown by $b_0$ = 500 and 1000 s/mm$^2$. Note that Std($b_0$ = 0) and T2wsup_with mask($b_0$ = 0) provided the best performance through the entire range of $b_n$. The SNR ratios to the Std($b_0$ = 0) at $b_n$ = 1500 s/mm$^2$ in six cases were 33.9 (1.00), 33.9 (1.00), 31.1 (0.92), 24.7 (0.73), 21.4 (0.63), and 9.8 (0.29) in a descending order. ADC, apparent diffusion coefficient; $b$, b-value; FLAIR, fluid attenuation inversion recovery; DWI, diffusion-weighted imaging; NBZ, non-$b$-zero; SE, spin-echo; SI, signal intensity; Std, standard; T2wsup, T2-based water suppression.

was nearly 50–80% for the NBZ compared with the current T2wsup (Fig. 8 and Table 3). This result was almost theoretically comparable with that of our simulation, as shown in Fig. 5. These results showed that the tissue SNRs were preserved (Table 3) even by subtraction because of the masked subtraction technique of this study.

Figures 9 and 10 show the results of the DTI in case 2. Comparing the Std and T2wsup images (Fig. 9) with those numerical results in the CSF-PVE portions (Fig. 10), the T2, MD, and FA values became close to pure tissue values, i.e., the T2 and MD became lower and the FA values became closer to 1 in the T2wsup images, typically at the portion of the fornix crus or genu of the corpus callosum where CSF-PVE was greater because of the ventricle. Furthermore, FT for the T2wsup method at the central portions of two seed ROIs was thicker and better connected than that for the Std DWI.

## Discussion

The currently proposed T2wsup–dMRI technique was assessed using the simulation of the current study and MRI *in vivo* study. Moreover, the currently proposed technique was demonstrated to sufficiently suppress the water signals in DWI images through the entire range of $b$, including $b$ = 0. Furthermore, the quantitative parameter values of T2, ADC (MD), and FA were demonstrated to be close to pure tissue values under certain limitations even when the CSF–PVE portions were included in the ROI or voxels. Moreover, the fiber tracts of the fornix were correctly visualized even in the CSF–PVE portions because the FA values for the T2wsup technique became greater than those for the Std (without wsup) method. The following section compared this technique with several alternative methods and discussed the modifications and future of the proposed technique.

### *Comparison between the T2wsup method and other alternative methods*

Regarding the comparison of the T2wsup method with the FLAIR method, CSF-PVE in FLAIR method was perfectly suppressed at the optimal TI, but the tissue SNR was lower in the FLAIR method than in our SE-based T2wsup method even using w/o masking, as shown in our theoretical simulation of $V_w$ = 0 (Table 2). In addition, it has been verified using MRI data that the T2wsup–$b_0$ images with masking have higher SNR than the FLAIR–$b_0$ images,[32] and that the ratio of SNR between the two methods is perceived to be independent of $b$.

When comparing the NBZ with our method, the SNR of ADC was roughly proportional to the difference of the two $b$, $b_0$ and $b_n$, in the two-point method if background noises were retained. Therefore, when $b_n$ is fixed and the water signal is ignored, the smaller the $b_0$, the better the SNR of ADC. In this case, the SNR of ADC for the NBZ method with $b_0$ = 500 s/mm$^2$ was 0.64 times that for the Std method with a $b_0$ value of 0 in this simulation. In addition, it is nearly 0.67 ([1500–500]/[1500–0]) times that of our method. Figure 8 shows that MD map with our T2wsup method is visually better than with the NBZ method because of the effects of keeping tissue SNRs on $b_0$ images between our T2wsup and the Std. Furthermore, the $b$ of approximately 500 s/mm$^2$ used in the NBZ was not sufficient because it required that a $b$ > 1000 s/mm$^2$ reduces the CSF signals almost perfectly (< 5%) in our results. The biggest advantage of our T2wsup method is that the entire range of $b$ (> 0) can be used to calculate the dMRI parameters without loss of tissue SNR.

In terms of the FWE method, although not compared yet, our T2wsup method has of imaging time and analysis simplicity if similar results can be provided. However, FWE method using a single-shell method can use a Std imaging protocol but requires multiple MPG directions; furthermore, some regularization techniques must be introduced to become robust because the original approach is ill-posed, resulting in poor tissue specificity due to smoothing effects.[16,17] The basic theory of separating free water and tissue in the FWE technique using a single-shell method is based on the assumptions that the free-water ADC is isotropic and having fixed value ($D_w$ = 3 × $10^{-3}$ mm$^2$/s). In contrast, our method can provide water-suppressed DWI images just using at least three different images (two $b$ = 0 and one $b$ > 0 with a single MPG direction) and does not require special analysis once T2wsup–$b_0$ images are obtained because our method is based

**Table 2** Noiseadded simulation results for $V_w$ = 0 (pure tissue signal) with 4 methods.

| Index | Parameter | DWI method ($b_0$,$b_1$) | | | |
|---|---|---|---|---|---|
| | | Std(0,1500) | T2wsup(0,1500) | NBZ(500,1500) | NBZ(1000,1500) |
| Ideal value | $T2_t$ (ms) | 100.0 | | NA | |
| | $\lambda_{t1}$ x $10^{-3}$ ($mm^2$/s) | | | 1.200 | |
| | $\lambda_{t2,\ t3}$ x $10^{-3}$ ($mm^2$/s) | | | 0.600 | |
| | $MD_t$ x $10^{-3}$ ($mm^2$/s) | | | 0.800 | |
| | $FA_t$ | | | 0.408 | |
| Mean | $T2_t$ (ms) | 100.15 | 100.19 | NA | |
| | $\lambda_{t1}$ x $10^{-3}$ ($mm^2$/s) | 1.201 | 1.202 | 1.201 | 1.203 |
| | $\lambda_{t2,\ t3}$ x $10^{-3}$ ($mm^2$/s) | 0.600 | 0.600 | 0.600 | 0.601 |
| | $MD_t$ x $10^{-3}$ ($mm^2$/s) | 0.801 | 0.801 | 0.800 | 0.801 |
| | $FA_t$ | 0.409 | 0.409 | 0.408 | 0.408 |
| SD | $T2_t$ (ms) | 1.37 | 1.37 | NA | |
| | $\lambda_{t1}$ x $10^{-3}$ ($mm^2$/s) | 0.041 | 0.041 | 0.063 | 0.138 |
| | $\lambda_{t2,\ t3}$ x $10^{-3}$ ($mm^2$/s) | 0.018 | 0.018 | 0.028 | 0.061 |
| | $MD_t$ x $10^{-3}$ ($mm^2$/s) | 0.0169 | 0.016 | 0.0249 | 0.0544 |
| | $FA_t$ | 0.0213 | 0.0214 | 0.0337 | 0.0733 |
| SNR | $T2_t$ (ms) | 73.08 | 73.22 | NA | |
| | $\lambda_{t1}$ x $10^{-3}$ ($mm^2$/s) | 29.23 | 29.30 | 18.94 | 8.70 |
| | $\lambda_{t2,\ t3}$ x $10^{-3}$ ($mm^2$/s) | 33.90 | 33.91 | 21.43 | 9.83 |
| | $MD_t$ x $10^{-3}$ ($mm^2$/s) | 47.37 | 47.37 | 32.14 | 14.73 |
| | $FA_t$ | 19.18 | 19.09 | 12.12 | 5.56 |

These simulated conditions where shown in Table 1. The tissue SNR was the same as in Fig. 4 . (SNR = 100 for SI [$TE$ = 100 ms, $b_0$ = 0]). Note that the SNR of each parameter in T2wsup method was almost the same as in the Std method and better than the two NBZ methods. The other parameters were the same as in Fig. 3. The major simulation parameters are shown in Table 1. The other parameters are: $ThVw_{min}$ = 0.1, SNR = 100 (SNR= S[TE = 100ms, b = 0]/$\sigma$). $b$, b-value; DWI, diffusion-weighted imaging; NBZ, non-$b$-zero; SD, standard deviation; SI, signal intensity; Std, standard; T2wsup, T2-based water suppression.

on just the T2 difference between free water and tissue. Furthermore, the water motion in the FWE method will introduce difficulty in separating water from the tissue components because the diffusion anisotropy of the CSF introduces a divergence from their model assuming stationary water.[8] In contrast, our T2wsup method is robust to water motion because it uses non-DWI ($b$ = 0) images for separating water and tissue.

More recently, a new wsup technique providing multiple T2 components of tissue, including water without using diffusion model, was proposed.[38] Their technique is similar to the T2wsup method of this study wherein the data on multi-TE with a single $b$ value were combined. However, the blind source separation technique without model assumption was used there. Furthermore, future assessments will need to be informative and usable whether with TE or $b$ or both for separating multiple tissue components in clinical use.

## *Modification of the proposed technique*

### Errors in quantitative parameters in T2wsup method and the solution

The simple analytical algorithm in the T2wsup method was applied to obtain several quantitative parameter maps by using minimum data of combining $TE$ and $b$. However, when $T2_t$ becomes long and/or $TE_{long}$ is not sufficiently long, errors in tissue T2 and $T2_t$ with the T2wsup method will be introduced. Therefore, errors in $MD_{wsup}$ and $FA_{wsup}$ become greater as shown in Fig. 6. The accuracies of the quantitative parameters in the proposed T2wsup method are almost decided in the T2wsup data of $b$ = 0. The use of longer $TE_{long}$ reduces the T2wsup errors even using the current algorithm to reduce the errors (Fig. 11). Moreover, the $TE_{long}$ of ~1,000 ms is not extremely unrealistic in the EPI sequence. A technique of masking with thresholding to reduce the problems associated with the fast-spin-echo (FSE)-based T2wsup technique has been proposed.[32] The

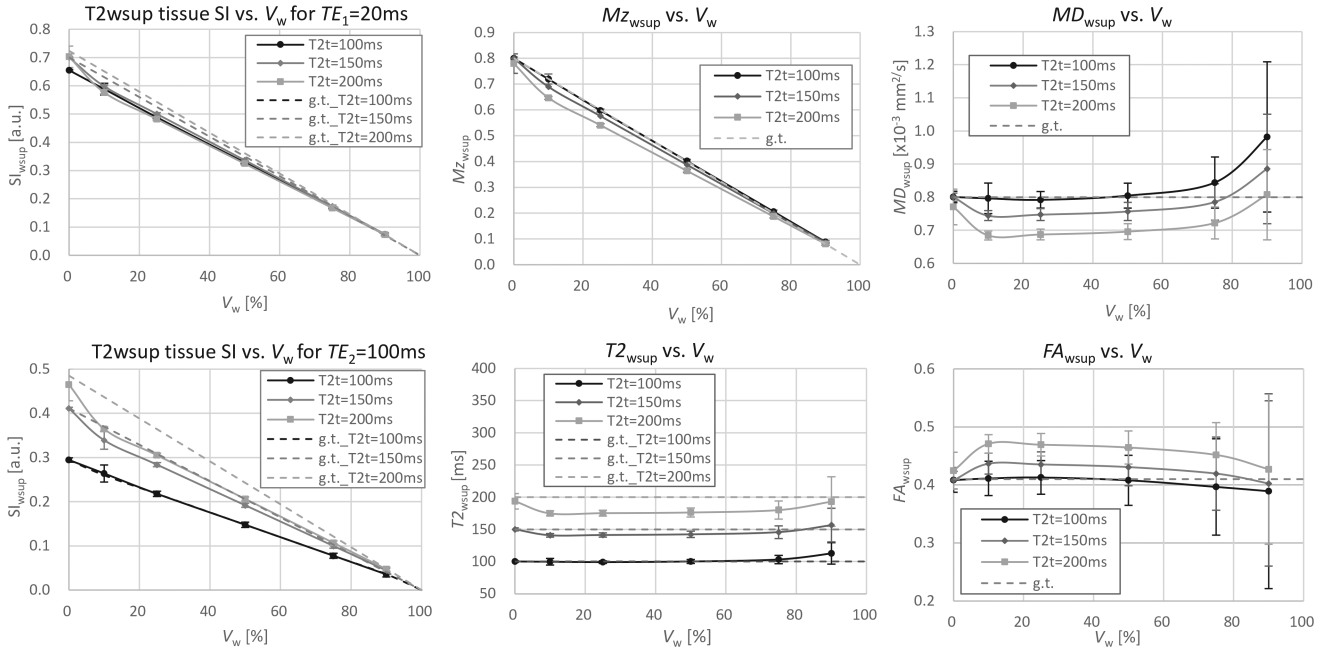


**Fig. 6** Noise added simulation results (mean ± SD) for water suppressed SIs for SE with 2 TE, and quantitative tissue parameters of Mz, T2, MD, and FA as parameters of water volume, $V_w$ (%) and tissue T2,$T2_t$ (ms), each obtained with T2wsup method under Rician noise of SNR=100 on SI ($TE$=100 ms, $b$=0, and $V_w$=0). Ground truth (g.t.) values were also shown. $TE_{long}$ was commonly 500 ms. All parameters for tissue ($T2_t$ =100ms) provided the tissue specific values except for $V_w$ =100 %, however those errors were increased with increasing $T2_t$. All errors at $V_w$=0 (pure tissue) were smaller because of the effects of the subtracting threshold with $ThVw_{min}$=10%. The SNRs in all parameters for T2wsup method became worse with increasing $V_w$ due to the lower tissue volume ($\propto Mz_t$) in a voxel. Other simulation parameters were shown in Table 1. *b*, b-value; FA, fractional anisotropy; g.t., ground truth; MD, mean diffusivity; Mz, magnetization; NBZ, non-*b*-zero; SD, standard deviation; SE, spin-echo; SI, signal intensity; T2wsup, T2-based water suppression.

very small $ThVw_{min}$ introduces tissue SNR reduction. By contrast, extremely large $ThVw_{min}$ introduces insufficient water suppression. The experiments with $TE_{long}$ = 300–500 ms and $ThVw_{min}$ = 0.1 for healthy volunteers provided reasonable results. Although it is difficult for the current T2wsup method with a similar $ThVw_{min}$ setting to perfectly preserve the accuracy when $V_w < 0$, subtracting tissue components can be less than the $ThVw_{min}$ (< 10% in this case).

Otherwise, nonlinear least square regression approach may be useful to simultaneously obtain unknown parameters of $T2_t$, $D_t$, and $Mz_t$ in the model equation defined by $S(TE, b)$ in Fig. 1 or in addition to the tensor model despite of computing cost and the number of image data. All FWE methods assumed that TE is constant. The number of data along the *b* axis may be reduced while maintaining the same accuracy or improving the accuracy of the obtained parameters if the FWE methods are extended to different TEs.

**Decay correction for water SI in DWI images**

Regarding the decay correction of water SI due to *b*, the computing cost is low; however, it is not always necessary that when the *b* is sufficiently high (e.g., $b > 1000$ s/mm$^2$), the water SI falls to < 5%. The correction for DWI images with greater *b* may not be performed because calculating ADC or FA correctly is impossible when the SI is negative or below Rician noise,[39] resulting in noise or requirements for masking.

CSF motion introduces the overestimation of water ADC, $D_w$ when it is assumed to be the value for stationary water. The portion of negative SI at the ventricle for a *b* of 250–500 mm$^2$/s in Fig. 6a was due to those effects. However, it is not an important problem because our T2wsup reduces the error in the ADC or FA maps due to CSF-PVE; those effects are major in the voxel of pure CSF portions but weak in the voxel of smaller $V_w$ because of slow CSF motion. If necessary, the portions of negative SIs are set to 0 after T2wsup correction. Applying a DWI sequence with a gradient moment nulling is desirable to reduce motion effects when the errors introduced using fixed $D_w$ are reduced.

***Applying to T2wsup–dMRI to synthetic MRI***

If the clinical purpose is only for dMRI with wsup, the additional data are only the long TE images in our T2wsup method. Current synthetic MRI is based on the

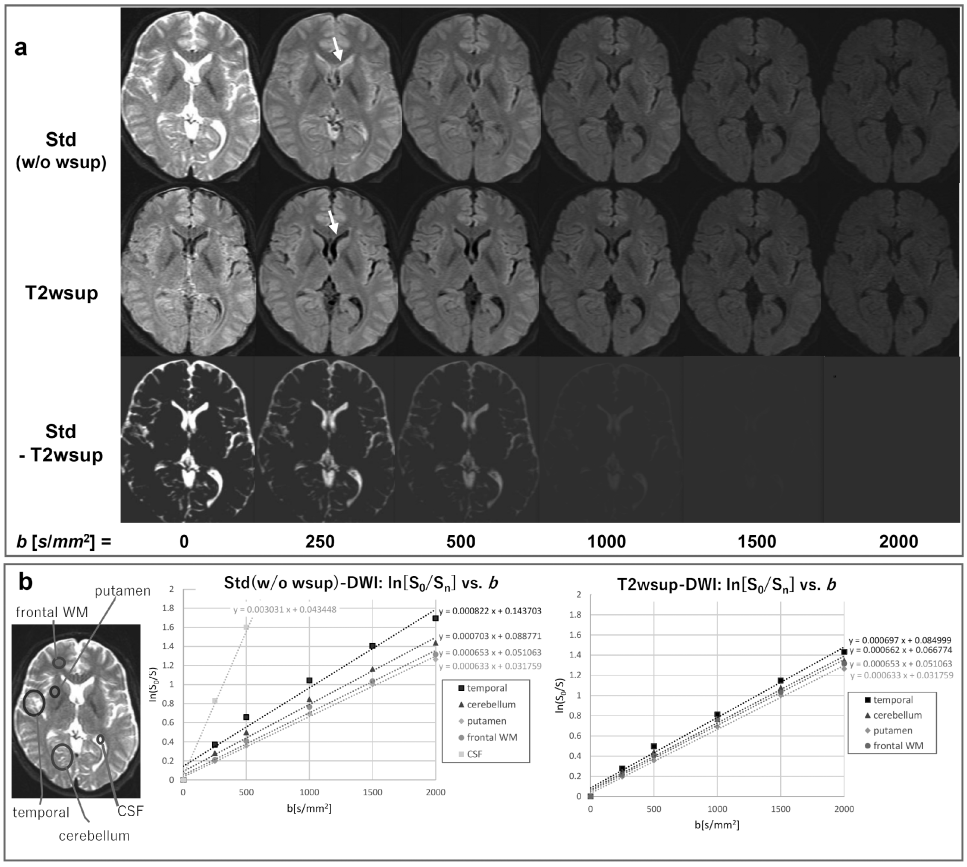


**Fig. 7** Healthy brain DWI imaging results for case 1. **a**: DWI images as a parameter of *b* for the Std (w/o wsup) method, our water suppression (T2wsup) method, and subtractions (Std – T2wsup) in case 1. Here, all images were shown with the same window level and width. The CSF signals in T2wsup were well suppressed even at small *b* (< 500 s/mm$^2$) (arrows), although the CSF signals in the Std and T2wsup methods were almost comparably decreased with the increasing *b* (> 1000 s/mm$^2$). Moreover, the tissue SNRs in the T2wsup method were maintained similarly to those in the Std method because of our masking technique. **b**: ROI analysis results for the Std (left) and T2wsup (right) methods, each shown by ln[*S*(*b*)] vs. *b* with linear fitting by ln[*S*(*b*)]= ln[*S*(*b*)] = *A* × *b* + *B*. The gradients *(A)* corresponding to the ADC or MD were increased in the cerebellum or temporal lobe and those *Bs* for Std were not zero, reflecting CSF–PVE, in the standard method. By contrast, the gradients became almost similar even at CSF–PVE ROIs, and the *Bs* became almost zero due to the effects of CSF suppression in the T2wsup method. The numerical values are shown in Table 3. ADC, apparent diffusion coefficient; *b*, b-value; CSF, cerebral spinal flood; DWI, diffusion-weighted imaging; MD, mean diffusivity; PVE, partial volume effect; Std, standard; T2wsup, T2-based water suppression; WM, white matter.

FSE sequence because the output is only T1, T2, and PD maps and contrast images with their combinations.[34–35] However, the advantages of combining T2wsup-dMRI with Std synthetic MRI are that the total MR acquisition time for a single patient is reduced and the comparison of different information becomes easier. The biggest advantage of this combined technique is obtaining CSF-PVE-free maps and images, particularly of FLAIR, almost the same as the FLAIR images obtained just by calculation. Finally, the CSF-PVE-free quantitative maps of PD, T1, T2, ADC, and FA and contrast images with an arbitral parameter combination of TR, TE, TI, and *b* were simultaneously obtained using the same anatomical positions.

### *Limitations*

Some limitations exist in applying the current technique to actual clinical use.

The first is the increased risk of insufficient wsup or errors in quantitative parameters for long T2 lesions depending on setting parameters in the proposed T2wsup algorithm as discussed above. Thus, the current method has to be carefully applied to actual clinical use. Moreover, how long tissue T2 must be supported in the actual clinical use of dMRI with water suppression must be separately made clear. Thereafter, better solutions are prepared depending on the issue of tissue T2.

The second is the increased risk of misregistration between $b_0$ and long TE images. Separate acquisitions of

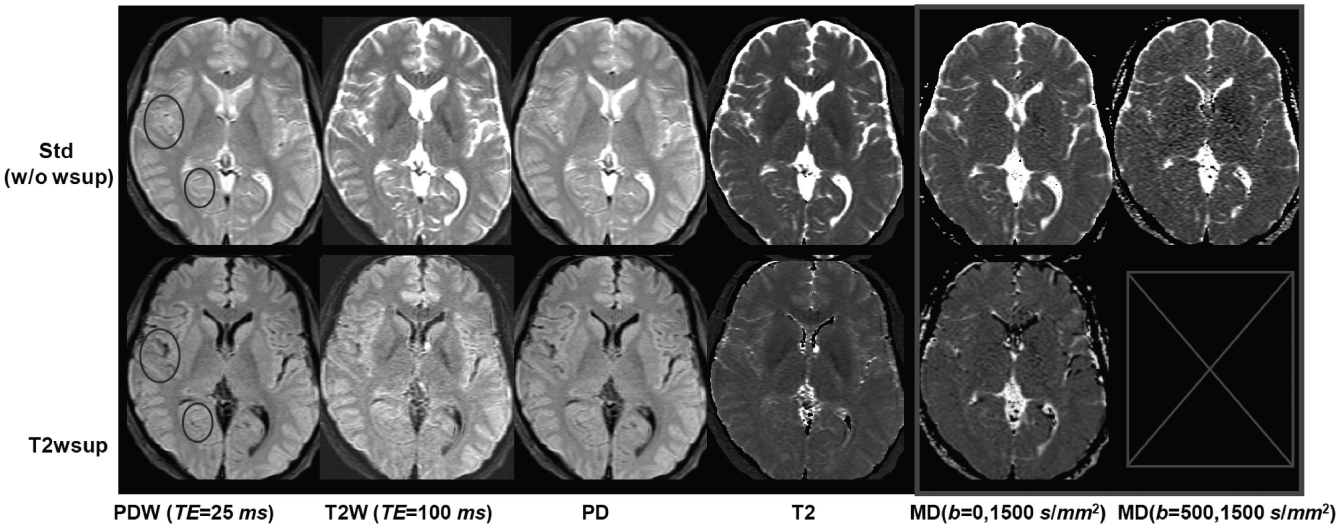


**Fig. 8** Contrast-enhanced weighted images and parameter maps for the Std (w/o wsup) method and our water suppression (T2wsup) method for case 1. The hyperintense artifacts due to the CSF-PVE shown in the Std method were well reduced in the T2wsup method, especially at the temporal cortex and cerebellum (circle ROIs). For MD maps, the CSF–PVE artifacts were reduced in the standard method with $b$ = 500 and 1,500 s/mm$^2$ corresponding to the NBZ method and persisted compared with those in the currently proposed T2wsup method with $b$ = 0 and 1,500 s/mm$^2$. The tissue SNRs for the T2wsup method with $b$ = 0 and 1,500 s/mm$^2$ were visually better than those for the standard method of $b$ = 500 and 1,500 s/mm$^2$ (NBZ), particularly in the center portion. ROI analysis results are shown in Table 3. *b*, b-value; CSF, cerebral spinal flood; MD, mean diffusivity; NBZ, non-*b*-zero; PD, proton density; PDW, proton density weighted image; PVE, partial volume effect; Std, standard; T2W, T2 weighted image; T2wsup, T2-based water suppression.

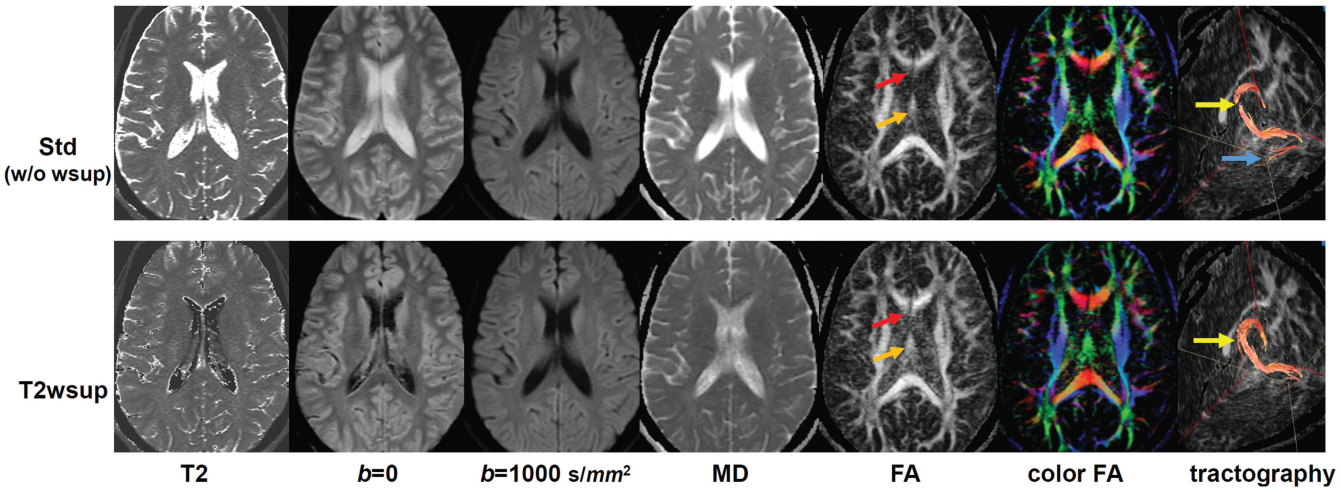


**Fig. 9** Comparison of DTI images, quantitative maps, and fiber tractographies, for standard (Std [w/o wsup]) and for our water suppression (T2wsup) in case 2. The T2wsup provided better tissue-specific values for the tissues close to the boundary regions of the ventricle, as the body of fornix (orange arrows), or genu of corpus callosum (red arrows). Those numerical values at several ROIs were shown in Fig. 10. For the tractographies of fornix, the fibers at the central portions of two seed ROIs (yellow arrows) for T2wsup was thicker and better connected than for the standard, and artifactual fibers were drawn for the standard (blue arrow). Here the FA threshold is commonly 0.25, and the seed ROIs were set at two positions of the top of the body on this slice and the right crus of fornix on the bottom axial slice (not shown). *b*, b-value; FA, fractional anisotropy; DTI, diffusion tensor imaging; MD, mean diffusivity; Std, standard; T2-based water suppression.

different TEs were used for the pulse sequence to obtain T2wsup images with $b$ = 0. A multiecho (> 2) EPI sequence may be desirable to make it robust against the misregistration artifacts in T2wsup–$b_0$ images and to reduce the total acquisition time.

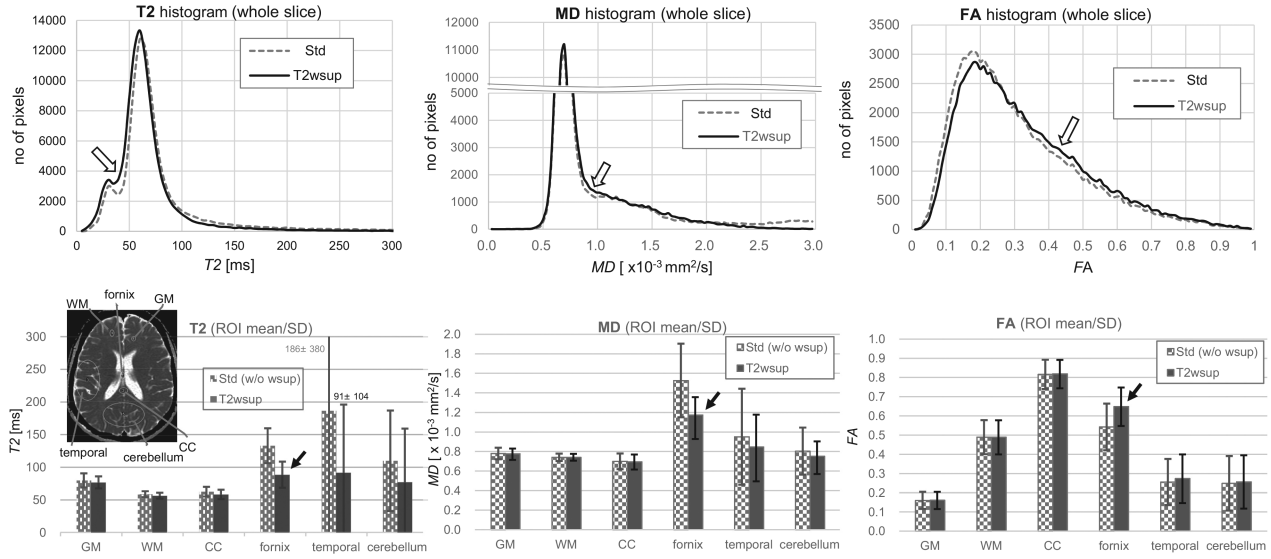


**Fig. 10** Histogram of whole slice (top) and the ROI analysis results (mean ± SD) (bottom) of T2, MD and FA for Std (w/o wsup) and water suppression (T2wsup) at several representative ROIs in case 2. The histograms of T2, MD and FA for T2wsup show the increase of the number of tissue specific pixels (thick arrows) compared with the standard. For the ROI analysis, the values of T2, MD and FA for T2wsup were respectively reduced, reduced and increased in fornix (open arrows), temporal lobe and cerebellum regions compared with those in the standard. By contrast, the pure tissue ROIs for CC, GM, and WM provide almost comparable values. CC, corpus callosum; FA, fractional anisotropy; GM, gray matter; MD, mean diffusivity; SD, standard deviation; Std, standard; T2wsup, T2-based water suppression; WM, white matter.

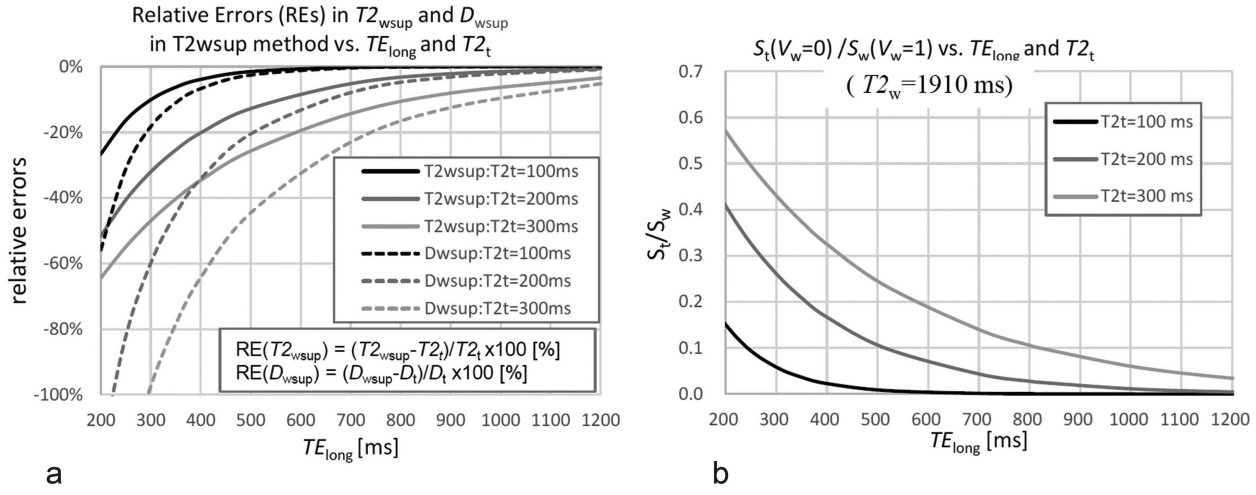


**Fig. 11 a:** REs in $T2_{wsup}$ and ADC ($D_{wsup}$) vs. $TE_{long}$ and $T2_t$ when using no thresholding with $ThVw_{min}$ ($ThVw_{min}$ = 1) in T2wsup method. The errors in the tissue T2 and ADC with T2wsup method become smaller with increasing $TE_{long}$ or decreasing $T2_t$. **b**: SI ratio of pure tissue ($V_w$ = 0) and pure water ($V_w$ = 1), $S_t/S_w$ vs. $TE_{long}$. The $S_t/S_w$ ratio corresponds to the maximum $ThVw_{min}$ to preserve the tissue signals w/o subtraction under the given $T2_t$ and $TE_{long}$ in our T2wsup method. For example, when $ThVw_{min}$ = 0.1, the minimum $TE_{long}$ (ms) values without errors were 243, 515, and 820, when $T2_t$ (ms) values are 100, 200, and 300, respectively, as shown in dotted vertical line. ADC, apparent diffusion coefficient; REs, relative errors; SI, signal intensity; T2wsup, T2-based water suppression.

### *Future*

Our technique is useful in reducing the number of different compartments in a multi-compartment model. The original model of intra-voxel coherent motion (IVIM)[40] assumes the two compartments of perfusion and diffusion. Here, perfusion is capillary flow, and diffusion includes stationary water and tissue when considering CSF-PVE (i.e., three compartments in a single voxel). Pure tissue is further divided into two components: fast and slow.[41] A recently proposed model of neurite

**Table 3** DWI ROI analysis results (mean ± SD) of T2, isotropic DWI SIs, and MD mm$^2$/s for Standard-DWI (**a**) and for T2wsup-DWI (**b**) in a volunteer study case 1.

| (a) Standard (w/o wsup)-DWI | | | | | | |
|---|---|---|---|---|---|---|
| Subject | Imaging parameters | CSF + tissue | | Tissue: GM | Tissue: WM | CSF 100% |
| | | Temporal | Cerebellum | Putamen | Frontal WM | Ventricle |
| *T2* (ms) | TE= (25, 80) (ms) | 101±76 | 71±14 | 53±3 | 57±2 | 1302±647 |
| DWI S.I. (a.u.) | *b* = 0 (s/mm$^2$) | 260.3±54.9 | 235.3±38.0 | 179.4±14.8 | 162.9±12.0 | 617.4±18.8 |
| | *b* = 250 | 179.7±24.3 | 177.8±17.4 | 147.5±5.1 | 132.1±8.6 | 268.9±15.5 |
| | *b* = 500 | 134.8±27.6 | 143.0±12.1 | 125.5±6.6 | 108.2±7.4 | 124.5±8.3 |
| | *b* = 1000 | 91.5±22.3 | 101.1±10.2 | 89.8±5.7 | 75.8±5.3 | 29.4±7.4 |
| | *b* = 1500 | 63.8±17.3 | 73.6±9.2 | 65.8±5.0 | 57.9±5.2 | 7.5±4.6 |
| | *b* = 2000 | 47.7±12.9 | 56.0±7.1 | 50.7±7.5 | 43.7±6.3 | 7.9±5.2 |
| *MD* with LSQ fitting (x10$^{-3}$ mm$^2$/s) | *b* = 0~2000: 6points | 0.85±0.23 | 0.66±0.064 | 0.64±0.07 | 0.66±0.06 | 1.17±0.58 |
| | *b* = 0~1000: 4points | 1.05±0.44 | 0.83±0.18 | 0.68±0.09 | 0.76±0.07 | 3.08±0.03 |
| | *b* =1000~2000: 3points | 0.61±0.19 | 0.58±0.10 | 0.58±0.28 | 0.56±0.12 | 1.78±1.83 |
| *MD* with 2-point (x10$^{-3}$ mm$^2$/s) | *b* = 0, 1500 | 0.96±0.34 | 0.78±0.16 | 0.67±0.07 | 0.69±0.05 | 3.10±0.05 |
| | *b* = 500, 1500 | 0.78±0.19 | 0.68±0.12 | 0.65±0.08 | 0.63±0.09 | 2.97±0.08 |
| (b) T2wsup-DWI | | | | | | |
| Subject | Imaging parameters | CSF + tissue | | Tissue: GM | Tissue: WM | CSF 100% |
| | | Temporal | Cerebellum | Putamen | Frontal WM | Ventricle |
| *T2* (ms) | TE = (25, 80) (ms) | 69±88 | 66±6 | 53±3 | 57±2 | NA |
| DWI S.I. (a.u.) | *b* = 0 (s/mm$^2$) | 199.5±40.2 | 199.8±21.4 | 179.4±14.8 | 162.9±12.0 | 74.6±47.5 |
| | *b* = 250 | 151.0±45.7 | 160.5±17.0 | 147.5±5.1 | 132.1±8.6 | 12.6±29.0 |
| | *b* = 500 | 121.2±40.6 | 136.7±14.1 | 125.5±6.6 | 108.2±7.4 | 3.4±17.5 |
| | *b* = 1000 | 88.5±25.3 | 99.3±11.1 | 89.8±5.7 | 75.8±5.3 | 2.4±9.9 |
| | *b* = 1500 | 63.1±17.9 | 73.3±9.5 | 65.8±5.0 | 57.9±5.2 | 1.5±4.9 |
| | *b* = 2000 | 47.7±13.0 | 56.0±7.1 | 50.7±7.5 | 43.7±6.3 | 6.8±5.2 |
| *MD* with LSQ fitting (x10$^{-3}$ mm$^2$/s) | *b* = 0~2000: 6points | 0.85±0.23 | 0.71±0.11 | 0.64±0.07 | 0.66±0.06 | NA |
| | *b* = 0~1000: 4points | 0.77±0.42 | 0.74±0.10 | 0.68±0.09 | 0.76±0.07 | NA |
| | *b* = 1000~2000: 3points | 0.60±0.22 | 0.58±1.02 | 0.58±0.28 | 0.56±0.12 | NA |
| *MD* with 2-point (x10$^{-3}$ mm$^2$/s) | *b* = 0, 1500 | 0.75±0.19 | 0.71±0.09 | 0.67±0.07 | 0.69±0.05 | NA |
| | *b* = 500, 1500 | 0.62±0.18 | 0.65±0.09 | 0.65±0.08 | 0.63±0.09 | NA |

These ROIs were the same as in Fig. 7. The ADC at pure CSF in the Standard was close to the literature free-water value of $3 \times 10^{-3}$ mm$^2$/s. Note that the ADC values at the CSF-PVE portions (cerebellum, temporal lobe) for the Standard including *b* = 0 were greater than the pure tissue (putamen, frontal WM) values (0.6~0.7×10−3 mm2/s), but those for T2wsup became close to the pure tissue values. LSQ fitting: least-square fitting using denoted number of b-value range data, 2-point: obtaind with two different b-value data. ADC, apparent diffusion coefficient; *b*, b-value; CSF, cerebral spinal flood; DWI, diffusion-weighted imaging; PVE, partial volume effect; SD, standard deviation; SIs, signal intencities; Std, standard; T2wsup, T2-based water suppression; WM, white matter.

orientation dispersion and density imaging (NODDI)[42] assumed three compartments, including isotropic water. Separating residual components is expected to be easier and more precise compared with the current approach if the free-water component can be separated in those models by combining it with the currently proposed technique.

## Conclusion

A new diffusion MRI technique called the T2wsup–dMRI was proposed and assessed for suppressing water signals based on T2 differences to more easily solve the problem of CSF–PVE artifacts in the current dMRI technique. This technique has higher SNR compared with other already proposed wsup techniques with FLAIR or NBZ. The currently proposed T2wsup–dMRI could be useful in clinical settings, although further optimization of the pulse sequence and processing techniques and clinical assessments, particularly for long T2 lesions, are required.

## Acknowledgements

We sincerely thank Yuki Takai, Hiroshi Kusahara, Ryo Shiroishi, and Hitoshi Kanazawa of Canon Medical Systems Corporation for supporting the data acquisition and analysis in this study. The preliminary report was shown in Kimura et al.'s study.[43]

## Conflicts of Interest

The authors declare no conflicts of interest.

## References

1. Basser PJ, Jones DK. Diffusion-tensor MRI: theory, experimental design and data analysis - a technical review. NMR Biomed 2002; 15:456–467.
2. Mori S, Zhang J. Principles of diffusion tensor imaging and its applications to basic neuroscience research. Neuron 2006; 51:527–539.
3. Jones DK, Cercignani M. Twenty-five pitfalls in the analysis of diffusion MRI data. NMR Biomed 2010; 23:803–820.
4. Vos SB, Jones DK, Viergever MA, et al. Partial volume effect as a hidden covariate in DTI analyses. Neuroimage 2011; 55:1566–1576.
5. Alexander AL, Hasan KM, Lazar M , et al. Analysis of partial volume effects in diffusion-tensor MRI. Magn Reson Med 2001; 45:770–780.
6. Pfefferbaum A, Sullivan EV. Increased brain white matter diffusivity in normal adult aging: relationship to anisotropy and partial voluming. Magn Reson Med 2003; 49:953–961.
7. Latour LL, Warach S. Cerebral spinal fluid contamination of the measurement of the apparent diffusion coefficient of water in acute stroke. Magn Reson Med 2002; 48:478–486.
8. Salminen LE, Conturo TE, Bolzenius JD, et al. Reducing csf partial volume effects to enhance diffusion tensor imaging metrics of brain microstructure. Technol Innov 2016; 18:5–20.
9. Kwong KK, McKinstry RC, Chien D, et al. CSF-suppressed quantitative single-shot diffusion imaging. Magn Reson Med 1991; 21:157–163.
10. Falconer JC, Narayana PA. Cerebrospinal fluid-suppressed high-resolution diffusion imaging of human brain. Magn Reson Med 1997; 37:119–123.
11. Zacharopoulos NG, Narayana PA. Selective measurement of white matter and gray matter diffusion trace values in normal human brain. Med Phys 1998; 25:2237–2241.
12. Papadakis NG, Martin KM, Mustafa MH, et al. Study of the effect of CSF suppression on white matter diffusion anisotropy mapping of healthy human brain. Magn Reson Med 2002; 48:394–398.
13. Bhagat YA, Beaulieu C. Diffusion anisotropy in subcortical white matter and cortical gray matter: changes with aging and the role of CSF-suppression. J Magn Reson Imaging 2004; 20:216–227.
14. Chou MC, Lin YR, Huang TY, et al. FLAIR diffusion-tensor MR tractography: comparison of fiber tracking with conventional imaging. AJNR Am J Neuroradiol 2005; 26:591–597.
15. Concha L, Gross DW, Beaulieu C. Diffusion tensor tractography of the limbic system. AJNR Am J Neuroradiol 2005; 26:2267–2274.
16. Salminen LE, Conturo TE, Laidlaw DH, et al. Regional age differences in gray matter diffusivity among healthy older adults. Brain Imaging Behav 2016; 10:203–211.
17. Baron CA, Beaulieu C. Acquisition strategy to reduce cerebrospinal fluid partial volume effects for improved DTI tractography. Magn Reson Med 2015; 73:1075–1084.
18. Pasternak O, Sochen N, Gur Y, et al. Free water elimination and mapping from diffusion MRI. Magn Reson Med 2009; 62:717–730.
19. Lee JE, Chung MK, Lazar M, et al. A study of diffusion tensor imaging by tissue-specific, smoothing-compensated voxel-based analysis. Neuroimage 2009; 44:870–883.
20. Metzler-Baddeley C, O'Sullivan MJ, Bells S, et al. How and how not to correct for CSF-contamination in diffusion MRI. Neuroimage 2012; 59:1394–1403.
21. Berlot R, Metzler-Baddeley C, Jones DK, et al. CSF contamination contributes to apparent microstructural alterations in mild cognitive impairment. Neuroimage 2014; 92:27–35.
22. Bergamino M, Pasternak O, Farmer M, et al. Applying a free-water correction to diffusion imaging data uncovers stress-related neural pathology in depression. Neuroimage Clin 2015; 10:336–342.
23. Albi A, Pasternak O, Minati L, et al. PharmaCog Consortium. Free water elimination improves test-retest reproducibility of diffusion tensor imaging indices in the brain: a longitudinal multisite study of healthy elderly subjects. Hum Brain Mapp 2017; 38:12–26.
24. Pasternak O, Shenton ME, Westin CF. Estimation of extracellular volume from regularized multi-shell diffusion MRI. Med Image Comput Comput Assist Interv 2012; 15(Pt 2):305–312.
25. Golub M, Neto Henriques R, Gouveia Nunes R. Free-water DTI estimates from single b-value data might seem plausible but must be interpreted with care. Magn Reson Med 2021; 85:2537–2551.
26. Blackledge MD, Leach MO, Collins DJ, et al. Computed diffusion-weighted MR imaging may improve tumor detection. Radiology 2011; 261:573–581.
27. Ueno Y, Takahashi S, Kitajima K, et al. Computed diffusion-weighted imaging using 3-T magnetic resonance imaging for prostate cancer diagnosis. Eur Radiol 2013; 23:3509–3516.

28. Kimura T, Machi Y. Computed Diffusion Weighted Imaging Under Rician Noise Distribution. Proceedings of the 20th Annual Meeting of ISMRM, Melbourne, 2012; 3574.
29. Kimura T, Machi Y, Kusahara H, et al. A short-TE Computed Diffusion Imaging (cDWI). Proceedings of the 23th Annual Meeting of ISMRM, Toronto, 2015; 2929.
30. Burdette JH, Elster AD, Ricci PE. Acute cerebral infarction: quantification of spin-density and T2 shine-through phenomena on diffusion-weighted MR images. Radiology 1999; 212:333–339.
31. Takai Y, Kimura T. Computed FLAIR-DWI Technique combined with DWI, PDW, T2W and T1W Images. Proceedings of the 24th Annual Meeting of ISMRM, Singapore, 2016; 3047.
32. Kimura T, Yamashita K, Fukatsu K. Synthetic MRI with T2-based Water Suppression to Reduce Hyperintense Artifacts due to CSF–Partial Volume Effects in the Brain. Magn Reson Med Sci 2021; 20:325–337.
33. Essig M, Deimling M, Hawighorst H, et al. Assessment of cerebral gliomas by a new dark fluid sequence, high intensity Reduction (HIRE): a preliminary study. J Magn Reson Imaging 2000; 11:506–517.
34. Warntjes JB, Leinhard OD, West J, et al. Rapid magnetic resonance quantification on the brain: Optimization for clinical usage. Magn Reson Med 2008; 60:320–329.
35. Tanenbaum LN, Tsiouris AJ, Johnson AN, et al. Synthetic MRI for Clinical Neuroimaging: Results of the Magnetic Resonance Image Compilation (MAGiC) Prospective, Multicenter, Multireader Trial. AJNR Am J Neuroradiol 2017; 38:1103–1110.
36. Bito Y, Hirata S, Yamamoto E. Optimal gradient factors for ADC measurements. Proceedings of the 3rd Annual Meeting of ISMRM. Nice, 1995; 913.
37. Xing D, Papadakis NG, Huang CL, et al. Optimised diffusion-weighting for measurement of apparent diffusion coefficient (ADC) in human brain. Magn Reson Imaging 1997; 15:771–784.
38. Molina-Romero M, Gómez PA, Sperl JI, et al. A diffusion model-free framework with echo time dependence for free-water elimination and brain tissue microstructure characterization. Magn Reson Med 2018; 80:2155–2172.
39. Gudbjartsson H, Patz S. The Rician distribution of noisy MRI data. Magn Reson Med 1995; 34:910–914.
40. Le Bihan D. What can we see with IVIM MRI? Neuroimage 2019; 187:56–67.
41. Maier SE, Mulkern RV. Biexponential analysis of diffusion-related signal decay in normal human cortical and deep gray matter. Magn Reson Imaging 2008; 26:897–904.
42. Zhang H, Schneider T, Wheeler-Kingshott CA, et al. NODDI: practical *in vivo* neurite orientation dispersion and density imaging of the human brain. Neuroimage 2012; 61:1000–1016.
43. Kimura T, Yamashita K, Fukatsu K. Synthetic-DWI with T2-based Water Suppression. Proceedings of the 29th Annual Meeting of ISMRM, Paris, 2020; 4386.